International Journal of Biological Macromolecules 154 (2020) 521–527

Contents lists available at ScienceDirect

International Journal of Biological Macromolecules

journal homepage: http://www.elsevier.com/locate/ijbiomac

Further insights into the evolution of starch assembly during retrogradation using SAXS

Lulu Zhang [a], Xiaoxi Li [a,*], Srinivas Janaswamy [b], Ling Chen [a], Chengdeng Chi [a,*]

[a] Ministry of Education Engineering Research Center of Starch and Protein Processing, Guangdong Province Key Laboratory for Green Processing of Natural Products and Product Safety, School of Food Science and Engineering, South China University of Technology, Guangzhou 510640, China
[b] Dairy and Food Science Department, South Dakota State University, Brookings, SD 57007, USA

ARTICLE INFO

Article history:
Received 14 February 2020
Received in revised form 28 February 2020
Accepted 15 March 2020
Available online 16 March 2020

Keywords:
Starch retrogradation
Molecular reassembly
SAXS
Amorphous structures
Ordered aggregate structures

ABSTRACT

A new and effective method for evaluating the reassembly of starch molecules at large scale (>2 nm) during retrogradation has been developed based on the small angle X-ray scattering (SAXS) technique. The SAXS curves fitted by the Cauchy plus Power-law functions are decomposed into peak- and non-peak-derived sub-patterns. The peak-derived patterns are used for calculating (i) the size of ordered aggregate structures (d) using Lorentz correction and (ii) the proportion of ordered structures within starch samples (R_{peak}) by estimating the ratio of the area under the peak-derived sub-pattern (S_{peak}) to the total area under SAXS curve. The I_{max} and fractal-like dimension (α) of the scattering aggregates (the fitted parameters of SAXS curve), d, S_{peak}, $S_{non\text{-}peak}$ (the area under the non-peak-derived sub-pattern) and R_{peak} change as a function of retrogradation time. Importantly, the $S_{non\text{-}peak}$ interrogates the continuous reduction of amorphous starch molecules during the aging, SAXS parameters including α and d describe starch ordered aggregate structures with larger scale than 2 nm are fitted well with pseudo Avrami equation. The SAXS in this study can be used to unravel the evolution of both amorphous starch structures and ordered aggregates with larger scale during retrogradation.

1. Introduction

Starch granules are organized at different length scales of structures, including whole granule (μm), growth rings (100–400 mm), lamellar structure (8–11 nm), crystallites (nm) and molecular assembly (~0.1 nm) [1–3]. These hierarchical structures get disrupted through gelatinization before human consumption as well as during starch-based functional materials development [4,5]. The disordered starch molecules, however, reassemble gradually into multi-scale structures in a process known as retrogradation [6]. Starch retrogradation is often considered to have undesirable effects on the quality of food products because the staling of starchy foods reduces shelf-life and consumer acceptance [7]. However, starch reassociation is desirable from the nutritional viewpoint due to the reduced starch digestion and lower postprandial glycemic response [8,9]. In this regard, knowledge on the starch reassembly during retrogradation needs to be established to understand the starch functionalities in starchy foods.

Starch retrogradation is a complex process involving a host of molecular and physicochemical changes [6]. For capturing the starch reassembling nature during this process, an array of analytical techniques, protocols and methodologies are being adapted. Those include Infrared spectroscopy [10,11], Raman spectroscopy [10], ^{1}H Nuclear Magnetic Resonance (NMR) [12], ^{13}C NMR [10,11], X-ray diffraction (XRD) [9] and Differential Scanning Calorimetry (DSC) [10,11] along with methods that focus on rheological, microscopic and physical properties of retrograded starches [6]. It is known that starch retrogradation involves with a drastic association of amorphous materials and in turn the formation of large reassemble units (>2 nm). However, classical techniques for evaluating starch retrogradation, e.g., DSC and XRD, are sensitive to helical and crystalline structures ranging from angstrom to nano-structures (<2 nm) [9,11,13], whilst there is lack of tools to evaluate the changes of amorphous starch and the formation of large reassemble units during retrogradation. Notably, how amorphous starch transforms and the large reassembled units reassociate during the retrogradation are the key factors influencing food digestibility and textural attributes [7–9]. That in turn stimulates interests in opening a new tool to identify correctly those structural changes for synergistically modulating digestion and eating quality of starchy foods.

Small angle X-ray scattering (SAXS) is being used for characterizing structural features of materials in the range of $0.001 < q < 5$ nm^{-1}, and thus making it as useful to unravel structures in a size range of several to hundreds nanometers [14,15]. There are several examples on studying the multi-scale structures of starches such as the amorphous

* Corresponding authors.
E-mail addresses: xxlee@scut.edu.cn (X. Li), c_cd124@163.com (C. Chi).

https://doi.org/10.1016/j.ijbiomac.2020.03.135
0141-8130/

lamellae (~3 nm), crystalline lamellae (~7 nm), semi-crystalline lamellae (~10 nm), aggregates (~10 nm), fractal structures (>10 nm) using SAXS [16–19]. Interestingly, in the case of starch, a strong scattering SAXS peak could be observed for the low-temperatures retrograded starch whilst no-peaks for that retrograded mildly at high temperatures [20], suggesting SAXS could be a viable technique to study the starch retrogradation. Nonetheless, the feasibility of evaluating starch reassembly kinetics based on the multi-scale structures (especially the structures with large reassemble units (>2 nm)) based on SAXS data has remained unsolved. This knowledge gap prompted us to undertake this study.

Herein, SAXS curves of retrograded starches were discussed with the potentials to reveal starch reassembly behavior during the retrogradation. The aggregation of amorphous starch and the formation of large reassemble units (>2 nm) such as fractal-like structures and ordered aggregates were extrapolated from SAXS data, to verify whether the SAXS data can reveal starch reassembly as a function of the retrogradation time. The outcome, indeed, reveals the evolution of starch assembly during retrogradation. To the best of our knowledge, this is the first study that discloses the reassembly kinetics of aging gelatinized starch by SAXS.

2. Materials and methods

2.1. Materials

Rice starch was purchased from Jinnong biotechnology Co., Ltd. (Jiangxi, China). The amylose content (ca. 13.2%) was determined using the iodine colorimetric method [21]. A moisture analyzer (MA35, Sartorius Stedim Biotech GmbH, Germany) was used to determine the moisture content (MC) of starch sample. The MC of the RS used for this study is found to be 13%.

2.2. Sample preparation

Rice starch was weighed accurately into a flask and mixed with 50 mL of distilled water to prepare starch suspension with a concentration of 20% (*w*/*v*). The suspension was fully gelatinized via cooking at boiling water with continuous stirring (300 rpm) for 30 min. After cooling to 25 °C, the starch paste was stored at 4 °C. The retrograded starch pastes after a desirable storage period at 4 °C were collected for SAXS analysis. The moisture content (ca. 60–70%) of starch gels were determined by the mass loss of starch gels after 12 h-oven drying at 110 °C [22]. In addition, retrograded samples were also freeze-dried for characterizing crystalline structure. The samples were stored at 4 °C for 0, 1, 3, 5 and 7 days and referred as RS-0, RS-1, RS-3, RS-5 and RS-7, respectively, for brevity, in the rest of the discussion.

2.3. X-ray diffraction (XRD)

The crystalline structures of starches were analyzed with an Xpert PRO diffractometer (Panlytical, Netherlands) operated at a current of 40 mA and voltage of 50 KV. Each sample was scanned with a Cu Kα radiation (λ = 0.1542 nm) in the 2θ range of 5 to 40° with a scanning step width of 0.033° and scanning speed of 10°/min. Initially, all the samples were equilibrated to 10% RH. The relative crystallinity (*RC*) was calculated as the ratio of crystalline region to the total diffraction area with PeakFit software (version 4.12, Inc. San Jose, USA) following the literature reported procedure [23].

2.4. Differential scanning calorimetry (DSC)

The thermal properties of starch samples were determined using a PerkinElmer DSC Diamond-I with an internal coolant (Intercooler 1P) and nitrogen purge gas. The rice starch granule suspension with a concentration of 30% (*w*/*v*) was added into a high-pressure stainless steel pan and covered with a gold-plated copper seal, then scanned from 30 to 100 °C with a heating rate of 10 °C /min. After this heating process, the pan with gelatinized starch was directly cooled to 25 °C and stored at 4 °C for suitable time. The starch pastes with 0, 1, 3, 5 and 7 days of storage at 4 °C were reheated from 30 to 100 °C with a heating rate of 10 °C /min. The enthalpy (Δ*H*) of starch gelatinization was calculated [24].

2.5. Small angle X-ray scattering (SAXS)

2.5.1. Sample determination

Small Angle X-ray Scattering (SAXS) measurements were carried out on SAXSess small-angle X-ray scattering system (Anton-Paar, Austria) which was equipped with a PW3830 X-ray generator (PANalytical) and Cu Kα radiation (λ = 0.1542 nm). The voltage and current were set as 40 kV and 50 mA, respectively. Native and retrograded rice starches were filled into a paste cell and exposed under the X-ray irradiation for 5 min. The data were recorded on an image plate and were collected by the IP Reader software using a PerkinElmer Storage Phosphor System. The paste cell without starch sample loading was used as a control for the background correction. The intensity was subtracted by background using SAXSquant 2D and SAXSquant 3.0 software [4]. All the data were normalized through adjusting the intensity at $q = 0$ to be 1 using SAXSquant 3.0 software. As the slit camera was used for SAXS detection, the data were also desmeared using SAXSquant 3.0 software. The processed data in the q (scattering vector) range of 1.15–1.5 nm^{-1} were collected for starch structural analysis.

2.5.2. Data analysis

The SAXS curves were fitted by the least square fitting according to the Eq. (1) [25]. The first term is given by the Cauchy function and describes the SAXS peak, while the second term is referred to the Power-law function and describes the underlying non-peak scattering.

$$I(q) = I_{max}\left[1 + 4\left(\frac{q-q_1}{\Delta q}\right)^2\right]^{-1} + Aq^{-\alpha} \quad (1)$$

herein, I_{max}, q_1, Δq (full width at half maximum) of the peak, A and α are positive adjustable parameters. Among those parameters, α can be used to calculate starch fractal-like structures. Based on previous studies [26–28], the scattering objects was characterized with a surface fractal structure if $3 < \alpha < 4$, whereas a mass fractal structure was described with a fractal dimension $D_m = \alpha$ if $1 < \alpha < 3$. A larger α indicated a higher compactness of the scattering objects [26].

Available studies have indicated that the density fluctuations from amorphous background materials and finite interface between crystalline and amorphous lamellae should be subtracted before analyzing lamellar parameters of semi-crystalline sample for improving the accuracy of SAXS parameters [29–31]. Zhang et al. [31] revealed that SAXS curve fitted by peak and non-peak sub-patterns can be used for analyzing starch lamellar structures with improved accuracy using the peak pattern decomposed from original SAXS curve. In order to accurately investigate the parameters of starch aggregate structures (e.g., the ratio of ordered or amorphous structure within starch, aggregate size (*d*)) of retrograded starch, the SAXS pattern was decomposed into peak and non-peak sub-patterns according to the Eq. (1), and then the area under the peak-derived sub-pattern (S_{peak}) and the area under the non-peak-derived sub-pattern ($S_{non\text{-}peak}$) were calculated [31] so as to obtain the ratio (R_{peak}) of ordered structures within each starch sample ($R_{peak} = S_{peak} / (S_{peak} + S_{non\text{-}peak})$) similar to the proportion (P_{SL}) of the semi-crystalline lamellae within starch granule (P_{SL} equates to the ratio of the net lamellar peak area to the total area of the SAXS pattern).

2.6. Statistical analysis

The data were statistically analyzed using IBM SPSS statistics version 21.0 (IBM, Armonk, NY, USA) and were presented as the mean ± standard deviation (±SD). Differences between groups were assessed by the analysis of variance, and $P < 0.05$ was considered to indicate a statistically significant difference among tests.

3. Results and discussion

3.1. Starch retrogradation behavior by XRD

The XRD patterns of starch samples are presented in Fig. 1. Native rice starch granules exhibited a typical A + V hybrid crystalline diffraction pattern with peaks at 15, 17, 18, 19.9 and 23.5° (2θ). However, after gelatinization followed by retrogradation, a combination of B- and V-type starch structure is noticed with apparent peaks at 17.1° (B-type) and 19.9° (V-type) along with feeble peaks at around 13 (V-type) and 23° (B-type). As the retrogradation time increased from 0 to 7 d, the intensity of characteristic peak of B-type structure at 23°(2θ) gradually increased. It is well known that the B-type crystals exist with arrangement of double helices. Thus, XRD results suggest upon retrogradation the content of starch double helical chains increased.

In order to unravel the changes of starch crystallinity during retrogradation, the XRD curves were fitted. The fitted curves were shown in Fig. S1 and the crystallinity were summarized in Table 1. The RS-0 had a *RC* of 13.1%, which is much lower than the rice starch of 33.2%. As the retrogradation time increased the *RC* gradually increases to 15.5%, portraying more B-type crystallites in the starch network are formed.

3.2. Retrogradation behavior by DSC

The gelatinization enthalpy (Δ*H*) of retrograded starch indicates the melting of crystals/double helices formed by amylopectin and/or amylose. The changes in Δ*H* of starch samples during storage at 4 °C are summarized in Table 1. Native rice starch granules had a Δ*H* of 10.38 J/g, which is much higher than the reassembled starches after retrogradation. This observation indicates that native rice starch had a more perfect and/or lager amount of crystallites or helical structures than that of reassembled starches. The RS-0 had a relatively low Δ*H* (0.18 J/g), suggesting a relatively weak of ordered reassembly of starch molecules when starch paste cooled to 25 °C temperature. As the aging time increased during the retrogradation, the Δ*H* slowly increased to 6.15 J/g, which meant that more energy is needed to melt the formed starch crystallites/ helices. Thus, it appears that extending the length of storage at 4 °C could likely to increase the ordered reassembly of starch molecules.

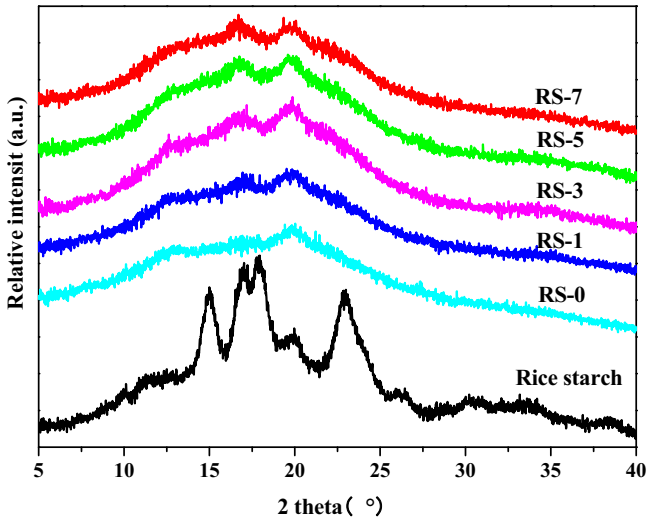

Fig. 1. X-ray diffraction patterns of native and retrograded starches.

3.3. Reassembly of retrograded starches as evaluated by SAXS

3.3.1. Qualitative analysis

SAXS has been actively used in analyzing starch amorphous, ordered and lamellar structures [4,17,18]. The SAXS curves from the study have been presented in Fig. 2. The rice starch had a scattering peak at ca. $q = 0.7\ nm^{-1}$, corresponding to starch semi-crystalline structure with an average lamellar thickness of ca. 9.0 nm (calculated from the Woolf-Bragg equation $d = 2\pi/q$). After cooking and cooling, this peak disappeared completely and a "shoulder-like" peak at ca. $q = 0.40\ nm^{-1}$ is observed, which is in line with reported results on starch cooking followed by storing that yields a "shoulder-like" peak at $q = 0.40\ nm^{-1}$ [15,32,33]. Lopez-Rubio et al. [15] and Li at al [33] indicated amylose and amylopectin after gelatinization would reassemble to form nanoscale molecular organizations (amorphous and/or ordered structure) during retrogradation. That in turn indicates that the appearance of "shoulder-like" peak witnessed starch reassembly and formed ordered aggregate structures after cooking and cooling. As shown in Fig. 2, the integrated area of this "shoulder-like" peak increases as a function of retrogradation time, further suggesting this peak involves with starch ordered reassembly structures during retrogradation. Hence, in this research, we resorted to analyze the "shoulder-like" peak ($q = 0.40\ nm^{-1}$) for understanding the evolution of starch reassembly during retrogradation.

This assumption is partially verified by the changes in SAXS intensity, especially that in low-*q* region. Based on the paracrystalline model of native starch granule [34], the SAXS intensity correlates to the electron contrast $\Delta\rho_u$ and $\Delta\rho$, where $\Delta\rho_u$ equals to the electron density difference between the amylose background region (ρ_u) and amylopectin amorphous lamella (ρ_a), $\Delta\rho$ equals to the electron density difference between the amylopectin crystalline lamella (ρ_c) and ρ_a. The increase in SAXS intensity in low-*q* region corresponds to the increase of $\Delta\rho_u$, while the increase in the overall SAXS intensity indicates the elevation of $\Delta\rho$. For retrograded starch, the sample similarly consists of three structures with different election density, i.e., amylose-based ordered region, amylopectin-based ordered region, and amylose/amylopectin amorphous region. Comparing with the amylopectin-based ordered region, amylose-based ordered region would be less densely-packed due to the limited content of amylose (13.2%). Accordingly, the amylopectin-based ordered region should be the most densely-packed structures followed by the amylose-based ordered region and amylose/amylopectin-based amorphous region. The SAXS intensity correlates with the election density difference of different densely-packed regions, i.e., $\Delta\rho_u$ equals to the electron density difference between the amylose-based ordered region (ρ_2) and the amylose/amylopectin-based amorphous region (ρ_3), $\Delta\rho$ equals to the electron density difference between the amylopectin-based ordered region (ρ_1) andρ_3. With an increase in $\Delta\rho$ and $\Delta\rho_u$, it contributes to an increase in overall SAXS intensity and the intensity in low-*q* region, respectively. During the short-term retrogradation, starch forms two regions including amylose-based ordered structures and amylose/amylopectin-based amorphous materials. With increasing the storage time, the short liner chains of amylopectin realign and long-term retrogradation occurs with formation of amylopectin-based ordered or crystalline region and amylose/amylopectin-based amorphous region. As can be seen from Fig. 2, the overall SAXS intensity, especially in low-*q* region, gradually increases as a function of the retrogradation time, indicating the continuous increase in the $\Delta\rho_u$ and $\Delta\rho$. The short chains of amylopectin would reassemble to form ordered aggregates during the long-term retrogradation, whilst, the ordered reassembly of amylopectin contributes to the reduction in amylopectin-based amorphous structures.

Table 1
Relative crystallinity (*RC*), enthalpy and SAXS fitting parameters of native and retrograded starches.[#]

Sample	*RC* (%)	Δ*H* (J/g)	Adj. R^2	I_{max}	α	$S_{non\text{-}peak}$	S_{peak}	R_{peak} (%)	q_1 (nm^{-1})	*d* (nm)
Rice starch	33.23 ± 0.71^a	10.38 ± 0.36^a	0.993	77.25 ± 1.24^e	2.61 ± 0.04^a	39.93 ± 3.57^f	32.97 ± 2.04^e	45.23 ± 0.35^d	0.7165 ± 0.003^a	8.77 ± 0.04^f
RS-0	13.15 ± 0.12^f	0.18 ± 0.05^f	0.999	39.50 ± 2.24^f	1.92 ± 0.02^d	94.51 ± 1.31^a	15.61 ± 1.66^f	14.18 ± 0.14^f	0.4986 ± 0.003^b	12.60 ± 0.08^e
RS-1	13.32 ± 0.13^e	3.55 ± 0.48^e	0.998	130.11 ± 3.43^d	2.27 ± 0.09^c	91.88 ± 1.62^b	54.79 ± 3.07^d	37.36 ± 0.44^e	0.4689 ± 0.007^c	13.50 ± 0.10^d
RS-3	13.76 ± 0.33^d	5.49 ± 0.22^d	0.995	255.64 ± 13.77^c	2.55 ± 0.16^b	86.88 ± 2.08^c	90.78 ± 4.38^c	51.10 ± 0.95^c	0.4127 ± 0.003^d	15.22 ± 0.12^c
RS-5	14.56 ± 0.52^c	5.83 ± 0.13^c	0.996	405.14 ± 11.89^b	2.56 ± 0.18^b	57.61 ± 2.19^d	116.88 ± 3.95^b	66.98 ± 0.84^b	0.3698 ± 0.007^e	17.00 ± 0.30^b
RS-7	15.58 ± 0.46^b	6.15 ± 0.14^b	0.996	494.61 ± 10.26^a	2.70 ± 0.17^a	52.89 ± 1.98^e	138.85 ± 2.77^a	72.42 ± 0.92^a	0.3467 ± 0.003^f	17.79 ± 0.17^a

[#] Values within column with different superscript letters are significantly different ($P < .05$).

Therefore, the change of $\Delta\rho$ could be as a result of increase of ρ_1 but decrease of ρ_3, while the increase in $\Delta\rho_u$ results from the increase or unchanged of ρ_2 but decrease of ρ_3. That in turn indicates the formation of amylose/ amylopectin-based ordered or crystalline structures, and meanwhile, the reduction of amorphous amylose/amylopectin branched-chains. This observation indicated that the evolution of the reassembly of amorphous amylose and amylopectin as well as the formation of ordered aggregate structures during retrogradation can be unraveled by the SAXS. The SAXS results could be used for analyzing the reassembly behavior of starch molecules during retrogradation and quantificational analysis of the evolution of ordered and amorphous structures is carried out in the following.

3.3.2. Quantificational analysis

In order to analyze the structural features of the retrograded starches by SAXS quantificationally, SAXS curves have been fitted by the Cauchy and Power-law functions [25]. The SAXS fitting parameters of the native and retrograded starches are shown in Table 1. The adjusted R^2 is higher than 0.99, indicating that SAXS curves could be well represented by the Cauchy and Power-law functions apart from the Power-law plus Gaussian functions [17,35]. The curve fittings of starch samples are shown in Fig. 3. It can be seen from Table 1 that the native rice starch had an I_{max} of 77.25 but the RS-0 had a much lower value of 39.50, due to disrupted starch granules by the hydrothermal treatment. However, after retrogradation at 4 °C, the I_{max} increases to 130.11, 255.64, 405.14 and 494.61 for 1, 3, 5 and 7 days, respectively, highlighting the starch ordered reassembly during the retrogradation. Based on a previous study [26], α could be used to evaluate the fractal-like structures of native and retrograded starches. All starches had a mass fractal structure in that the α was larger than 1 but smaller than 3. The rice starch has a α value of 2.61 and RS-0 of 1.92. In the retrograded starches, the value increases to 2.27, 2.55, 2.56 and 2.70 for 1, 3, 5 and 7 days, respectively, of retrogradation. In other words, it could be inferred that the compactness increases with the prolonged retrogradation [32]. Overall, the variations in α clearly accentuate the important fact that SAXS could be a valuable tool to monitor structural transformations in starches and to understand the extent of retrogradation.

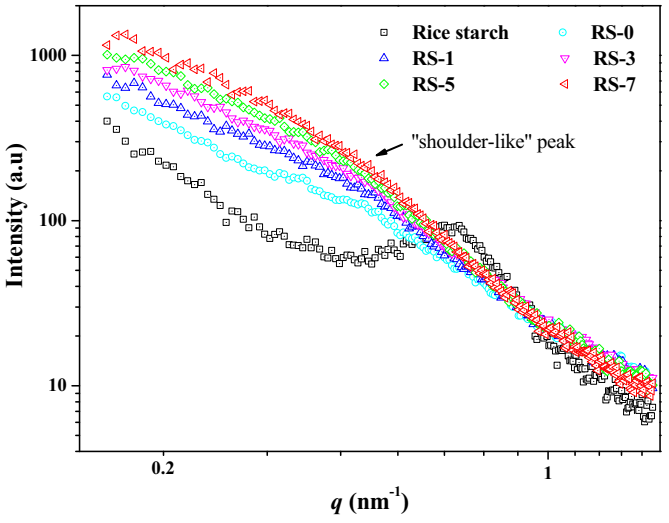

Fig. 2. SAXS curves of native and retrograded starches.

As the SAXS curves have been fitted by the Cauchy and Power-law functions, which are correlated to the SAXS peak and non-peak regions, the peak (ordered structures) and non-peak sub-patterns (amorphous regions) could be decomposed. Subsequently, the ratio of ordered structure in starch sample (R_{peak}) can be calculated from the area under the peak-derived sub-pattern (S_{peak}) and the area under the non-peak-derived sub-pattern ($S_{non\text{-}peak}$) ($R_{peak} = S_{peak} / (S_{peak} + S_{non\text{-}peak})$). The decomposed curves for native and retrograded starches are shown in Fig. 3, and the S_{peak}, $S_{non\text{-}peak}$, and R_{peak} are listed in Table 1. The RS-0 had a much higher $S_{non\text{-}peak}$ of 94.51 and lower S_{peak} of 15.61 and R_{peak} of 14.18 than the rice starch granules of 39.93, 32.97 and 45.23%, respectively, in the same order, indicating a progressive disruption of starch upon hydrothermal treatment. Increasing the retrogradation time has resulted in a continuous reduction in $S_{non\text{-}peak}$ along with an increase in S_{peak} and R_{peak} values. These changes could be due to the rearrangement of the starch chains during storage that further augments the increase of ordered structures and reduction of amorphous structures, which readily reflects in the SAXS curves.

In the retrogradation process, rearrangement of starch chains occur which induces changes in the size of starch ordered aggregate structure. According to a previous study [31], analyzing the starch ordered structures using peak curves decomposed from original SAXS profiles tend to improve the accuracy of the results. In this study, peak-derived sub-patterns (Fig. 4A) were used for calculating the size of starch ordered aggregate structure. Native starch had a peak at ca. 0.7 nm^{-1} over the curve, corresponding to the semi-crystalline lamellar structure with a size of ca. 9.0 nm. Cooked and retrograded starch showed a peak in the *q*-region lower than 0.7 nm^{-1}. Besides, the peak position moved from high *q*-region to low *q*-region as a function of retrogradation time (shown as grey dash line in Fig. 4A), indicating the size of ordered aggregate structure gradually increased during the retrogradation. This observation was in line with the starch reassembly behavior, i.e., the rearrangement of amylose and amylopectin aggregates, during the retrogradation. For identifying the peak position apparently, Lorentz transformation ($I^*q^2 \sim q$) of the data was used. The Lorentz-corrected patterns from original and peak curve data were shown in Fig. S2 and Fig. 4B, respectively. Both figures showed similar changes in the peak, i.e., the position moved to low-*q* region and the peak area increased as a function of aging time, indicating Lorentz-corrected peak curves could accurately unravel the changes of starch aggregate structure. Comparing with Fig. S2, Fig. 4B showed a higher peak definition with a distinguishable peak position. That further verified that analyzing starch structures using peak-derived sub-patterns significantly improved the accuracy. Table 1 showed the peak position (q_1) and the aggregate size (*d*) from Fig. 4B. Native rice starch had a smaller size of ordered aggregate structure than that of the gelatinized and retrograded starches, indicating hydrothermal treatment disrupts starch original ordered semi-crystalline lamellae but a suitable cooling

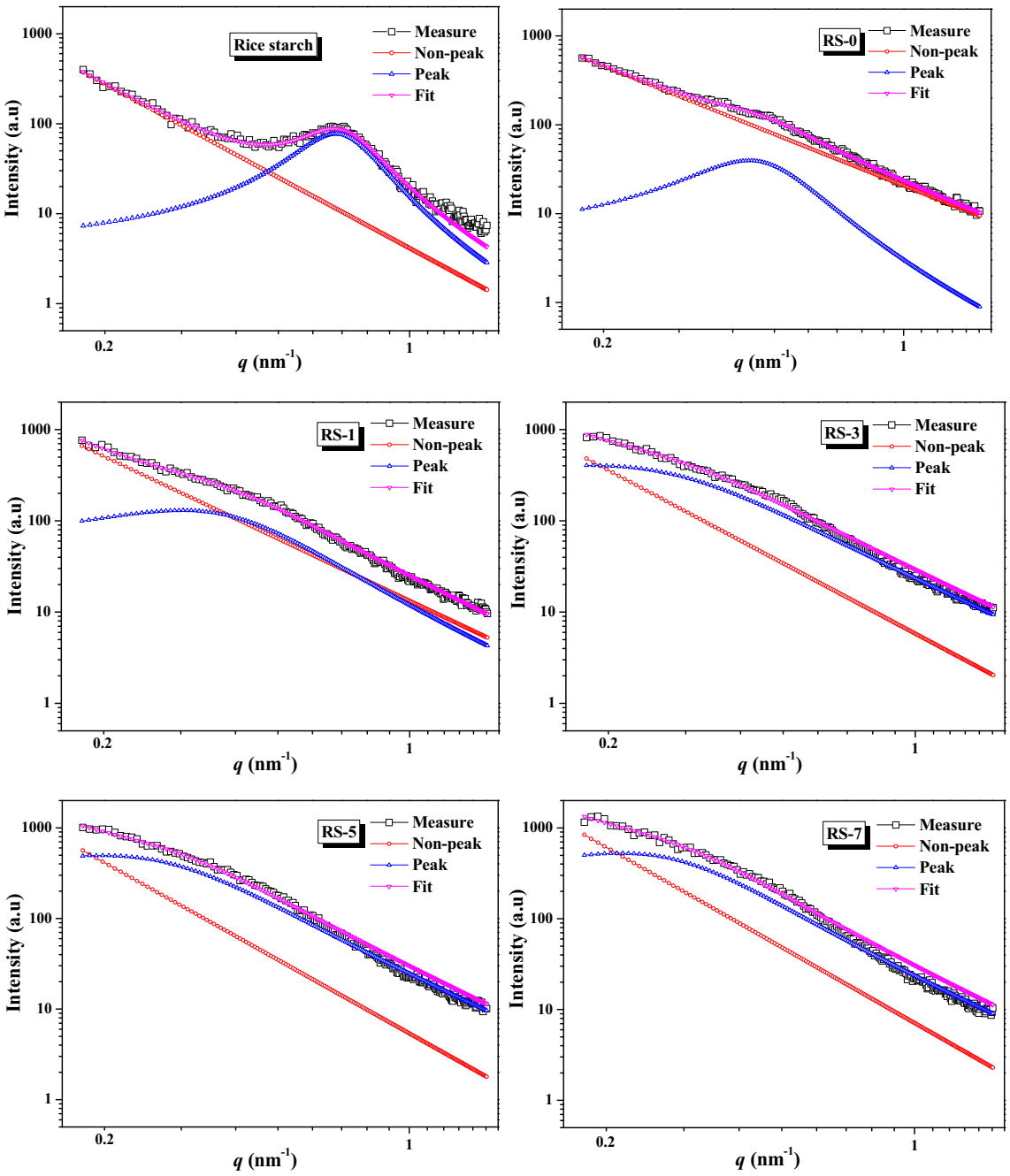

Fig. 3. Starch SAXS patterns and their fit curves.

assisted the rearrangement of ordered aggregates. During prolonged storage time at 4 °C, retrograded starches exhibit an increase in the size of ordered aggregate structure. This clearly indicates reassembly nature of starch molecules to form ordered structures during the storage. Overall, starch structural parameters calculated from the SAXS curves could be suitable to reveal the evolution of starch reassembly during retrogradation.

3.4. Evaluation the evolution of starch assembly during retrogradation

The rate and extent of starch retrogradation is associated with starch reorganization, nucleation and crystallites growth [36]. To reveal the kinetic changes in the ordered/crystalline structures of retrograded starches, Avrami equation is used extensively [6,9,13]. The general form of Avrami equation is as follows.

$$\frac{\Delta H_\infty - \Delta H_t}{\Delta H_\infty - \Delta H_o} = e^{-kt^n} \tag{2}$$

wherein ΔH_∞ is the limiting starch enthalpy, ΔH_o is the initial starch enthalpy, ΔH_t is the enthalpy of starch sample which has retrograded at time t, n is the Avrami exponent, and k is the rate constant. The rate constant (k) depends on the crystal nucleation and growth rate, and the n correlates with the crystal dimension [37]. As shown in Table 2, the experimental ΔH fits well with the Avrami model with a high determination coefficient ($R^2 = 0.999$). This indicates that the gelatinized starch was reassembled in a behavior obeying Avrami model. The XRD results,

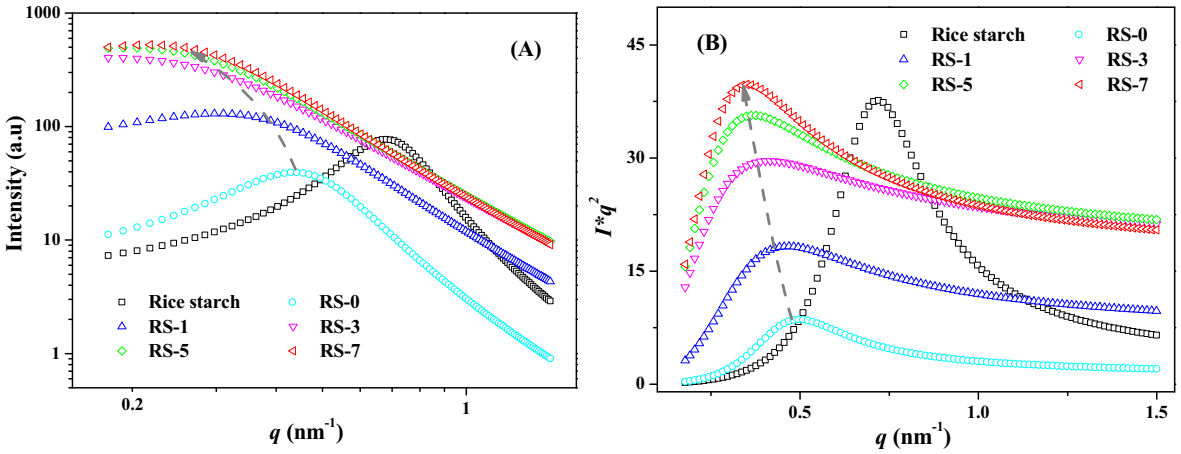

Fig. 4. Peak curves (A) and their Lorentz transformation (B) of SAXS patterns of native and retrograded starches. The grey dash lines indicated the changes of peak position.

especially the *RC*, also fits with relatively high fitting coefficient (R^2 = 0.980). The *k* and *n* values based on the Δ*H* and *RC* showed a significant difference. This is not surprising due to the fact that DSC and XRD evaluate different structural features of starch, i.e., DSC reveals melting of starch double or single helical structures while XRD unveils the starch crystalline architecture.

In the retrogradation process, the amorphous gelatinized starch reassociates into multi-scale ordered structures during retrogradation, and in turn forming crystallites composed of single or double helices that could be evidenced with DSC and XRD analysis. Increasing the retrogradation time, starch molecules reassemble in a larger scale (i.e., the size of structure is larger than 2 nm) and results in increased *RC* and Δ*H*. The SAXS reveals the multi-scale structural features of retrograded starches, and reveals that the dimension of starch fractal-like structure (i.e., the compactness of starch scattering aggregates), the proportion of ordered aggregate structures within retrograded starches, and the size of ordered aggregate structure continuously increase with increasing retrogradation time. Whilst, the proportion of amorphous structure gradually reduces as shown the changes of $S_{non\text{-}peak}$. That in turn indicates that the SAXS parameters can monitor starch molecular reassembly during retrogradation. Furthermore, this study aims to assess the possibility to evaluate the reassembly of starch aggregates (>2 nm) during retrogradation. Among the SAXS parameters, only fractal-like structure (α) and ordered aggregate structure (*d*) describe starch structures with a size larger than 2 nm, whilst, the proportion of ordered aggregate structures additionally correlated with structures smaller than 2 nm. Thus, the SAXS parameters, i.e., α and *d*, were fitted using pseudo Avrami mode (Eq. (3)) for revealing the kinetic reassembly of those starch structures.

$$\frac{X_\infty - X_t}{X_\infty} - X_o = e^{-kt^n} \tag{3}$$

wherein X_∞, X_o, and X_t are the limiting value, initial value, and the time-dependent value of starch SAXS parameters, respectively. The rate constant (*k*) depends on the reassembly and growth rate of starch reassembled structures, and the pseudo Avrami exponent (*n*) correlates with the dimension of aggregates. The fitting parameters of SAXS results based on pseudo Avrami Eq. (3) are shown in Table 2. α and *d* are all fitted well (with fitting coefficients are higher than 0.980), indicating the changes of these parameters obeying the pseudo Avrami model during starch retrogradation. It is noted that the *k* and *n* obtained from such SAXS parameters are significantly different because these parameters describe starch different structures at different scale.

Table 2
Fitting parameters of Avrami or pseudo Avrami equation based on DSC, XRD, and SAXS results.

	Δ*H*	*RC*	α	*d*
k	0.837 ± 0.029	0.039 ± 0.018	0.628 ± 0.097	0.129 ± 0.025
n	0.842 ± 0.047	1.923 ± 0.324	0.729 ± 0.148	1.529 ± 0.143
Adj. R^2	0.999	0.980	0.981	0.994

According to previous studies [7,38], the reassembly of amorphous amylose and amylopectin within the gelatinized starch system significantly correlated with foods eating quality, especially the gel structure and textural attributes of gluten-free foods. Starch reassembly contributes to the formation of food gel structure and in turn improves food textural attributes, however, an excess of reassembly of starch amorphous structure inevitably deteriorates food textural attributes because of the progressively-reassembled amorphous amylose and amylopectin and the increase in foods hardness [38]. That indicates that the ratio of amorphous starch fraction within foods associates with foods textural properties. On the other hand, structural features of reassembled starch also involve with starch digestibility. According to our previous studies [24,39–41], ordered aggregate structure and compactness (α) of fractal structure of the reassembled gelatinized starch significantly correlate with the content of slowly digestible starch (SDS) and resistant starch (RS). A highly-reassembled starch contains more ordered structure and a higher α value thereby significantly increases the SDS and RS content. Accordingly, the reassembly behaviors of gelatinized starch during retrogradation significantly correlate with food textural and nutritional attributes. However, the changes of starch digestibility are usually not accommodated with that of textural features. How to accommodate the changes of textural features with digestibility properties have yet to be resolved in the future. This study provides a potential way to unravel the reassembly of amorphous starch molecules and the evolution of ordered structure formation during retrogradation, which is of help to synergistically improve digestion and textural attributes of starchy foods.

4. Conclusion

This study reports use of SAXS data to understand the evolution of starch molecular reassembly during retrogradation. The SAXS profiles of retrograded starch can be fitted well using the Cauchy and the Power-law functions to obtain the SAXS peak and non-peak profiles as well as the parameters of I_{max} and α. In addition, S_{peak}, $S_{non\text{-}peak}$, R_{peak}, *d* could be accurately calculated from the sub-patterns. I_{max}, α, S_{peak}, R_{peak}, and *d* increased while $S_{non\text{-}peak}$ decreased as a function of retrogradation time, indicating those SAXS parameters correlate starch retrogradation. More importantly, α and *d* that describe starch aggregate structures larger than 2 nm are fitted well with pseudo Avrami equation. The SAXS parameters, e.g., α, *d*, S_{peak}, $S_{non\text{-}peak}$, and R_{peak}, can be

used for evaluating the reassembly of starch large ordered aggregates (>2 nm) and the reassembly of amorphous starch molecules during the retrogradation, providing a promising pathway to reveal starch reassembly behaviors that synergistically correlate with digestibility and textural attributes of starchy foods.

CRediT authorship contribution statement

Lulu Zhang: Visualization, Investigation, Software, Writing - original draft.**Xiaoxi Li:**Conceptualization, Methodology, Data curation, Funding acquisition, Writing - review & editing.**Srinivas Janaswamy:**Writing - review & editing.**Ling Chen:**Supervision, Project administration. **Chengdeng Chi:**Conceptualization, Methodology, Software, Validation, Writing - review & editing.

Acknowledgements

The authors thank the financial support from the National Key Research and Development Program of China (2016YFD04012021), the NSFC (31771930, 31271824), YangFan Innovative and Entrepreneurial Research Team Project (2014YT02S029), and the Fundamental Research Funds for the Central Universities. SJ thanks support from the USDA National Institute for Food and Agriculture (HATCH project SD00H648-18).

Appendix A. Supplementary data

Supplementary data to this article can be found online at https://doi.org/10.1016/j.ijbiomac.2020.03.135.

References

[1] A. Buleon, P. Colonna, V. Planchot, S. Ball, Starch granules: structure and biosynthesis, Int. J. Biol. Macromol. 23 (2) (1998) 85–112, https://doi.org/10.1016/s0141-8130(98)00040-3.
[2] W.-C. Liu, P.J. Halley, R.G. Gilbert, Mechanism of degradation of starch, a highly branched polymer, during extrusion, Macromolecules 43 (6) (2010) 2855–2864, https://doi.org/10.1021/ma100067x.
[3] S. Pikus, Small-angle x-ray scattering (SAXS) studies of the structure of starch and starch products, Fibres & Textiles in Eastern Europe 13 (5) (2005) 82–86.
[4] C. Chi, X. Li, Y. Zhang, L. Chen, L. Li, Understanding the mechanism of starch digestion mitigation by rice protein and its enzymatic hydrolysates, Food Hydrocoll. 84 (2018) 473–480, https://doi.org/10.1016/j.foodhyd.2018.06.040.
[5] S. Wang, L. Copeland, Molecular disassembly of starch granules during gelatinization and its effect on starch digestibility: a review, Food Funct. 4 (11) (2013) 1564–1580, https://doi.org/10.1039/c3fo60258c.
[6] S. Wang, C. Li, L. Copeland, Q. Niu, S. Wang, Starch retrogradation: a comprehensive review, Compr. Rev. Food Sci. F. 14 (5) (2015) 568–585, https://doi.org/10.1111/1541-4337.12143.
[7] F. Aguirre Juan, A. Osella Carlos, R. Carrara Carlos, D. Sánchez Hugo, P. Buera María del, Effect of storage temperature on starch retrogradation of bread staling, Starch - Stärke 63 (9) (2011) 587–593, https://doi.org/10.1002/star.201100023.
[8] M. Miao, B. Jiang, S.W. Cui, T. Zhang, Z. Jin, Slowly digestible starch–a review, Crit. Rev. Food Sci. Nutr. 55 (12) (2015) 1642–1657, https://doi.org/10.1080/10408398.2012.704434.
[9] M. Miao, B. Jiang, T. Zhang, Effect of pullulanase debranching and recrystallization on structure and digestibility of waxy maize starch, Carbohydr. Polym. 76 (2) (2009) 214–221, https://doi.org/10.1016/j.carbpol.2008.10.007.
[10] A. Flores-Morales, M. Jiménez-Estrada, R. Mora-Escobedo, Determination of the structural changes by FT-IR, Raman, and CP/MAS 13C NMR spectroscopy on retrograded starch of maize tortillas, Carbohydr. Polym. 87 (1) (2012) 61–68, https://doi.org/10.1016/j.carbpol.2011.07.011.
[11] X. Lian, C. Wang, K. Zhang, L. Li, The retrogradation properties of glutinous rice and buckwheat starches as observed with FT-IR, 13C NMR and DSC, Int. J. Biol. Macromol. 64 (2014) 288–293, https://doi.org/10.1016/j.ijbiomac.2013.12.014.
[12] G.M. Bosmans, B. Lagrain, E. Fierens, J.A. Delcour, The impact of baking time and bread storage temperature on bread crumb properties, Food Chem. 141 (4) (2013) 3301–3308, https://doi.org/10.1016/j.foodchem.2013.06.031.
[13] Y. Tian, Y. Li, F.A. Manthey, X. Xu, Z. Jin, L. Deng, Influence of β-cyclodextrin on the short-term retrogradation of rice starch, Food Chem. 116 (1) (2009) 54–58, https://doi.org/10.1016/j.foodchem.2009.02.003.
[14] J. Blazek, E.P. Gilbert, Application of small-angle X-ray and neutron scattering techniques to the characterisation of starch structure: a review, Carbohydr. Polym. 85 (2) (2011) 281–293, https://doi.org/10.1016/j.carbpol.2011.02.041.
[15] A. Lopez-Rubio, A. Htoon, E.P. Gilbert, Influence of extrusion and digestion on the nanostructure of high-amylose maize starch, Biomacromolecules 8 (5) (2007) 1564–1572, https://doi.org/10.1021/bm061124s.
[16] C. Chi, X. Li, Y. Zhang, L. Chen, L. Li, Z. Wang, Digestibility and supramolecular structural changes of maize starch by non-covalent interactions with gallic acid, Food Funct. 8 (2) (2017) 720–730, https://doi.org/10.1039/c6fo01468b.
[17] Z. Yang, Q. Gu, E. Lam, F. Tian, S. Chaieb, Y. Hemar, In situ study starch gelatinization under ultra-high hydrostatic pressure using synchrotron SAXS, Food Hydrocoll. 56 (2016) 58–61, https://doi.org/10.1016/j.foodhyd.2015.12.007.
[18] Q. Kuang, J. Xu, Y. Liang, F. Xie, F. Tian, S. Zhou, X. Liu, Lamellar structure change of waxy corn starch during gelatinization by time-resolved synchrotron SAXS, Food Hydrocoll. 62 (2017) 43–48, https://doi.org/10.1016/j.foodhyd.2016.07.024.
[19] B. Zhang, Y. Zhao, X. Li, L. Li, F. Xie, L. Chen, Supramolecular structural changes of waxy and high-amylose cornstarches heated in abundant water, Food Hydrocoll. 35 (2014) 700–709, https://doi.org/10.1016/j.foodhyd.2013.08.028.
[20] K. Shamai, E. Shimoni, H. Bianco-Peled, Small angle X-ray scattering of resistant starch type III, Biomacromolecules 5 (1) (2004) 219–223, https://doi.org/10.1021/bm034332i.
[21] X. Tan, X. Li, L. Chen, F. Xie, L. Li, J. Huang, Effect of heat-moisture treatment on multi-scale structures and physicochemical properties of breadfruit starch, Carbohydr. Polym. 161 (2017) 286–294, https://doi.org/10.1016/j.carbpol.2017.01.029.
[22] C. Chi, X. Li, Y. Zhang, S. Miao, L. Chen, L. Li, Y. Liang, Understanding the effect of freeze-drying on microstructures of starch hydrogels, Food Hydrocoll. (2019) 105509. doi:https://doi.org/10.1016/j.foodhyd.2019.105509.
[23] A. Lopez-Rubio, B.M. Flanagan, E.P. Gilbert, M.J. Gidley, A novel approach for calculating starch crystallinity and its correlation with double helix content: a combined XRD and NMR study, Biopolymers 89 (9) (2008) 761–768, https://doi.org/10.1002/bip.21005.
[24] C. Chi, X. Li, P. Lu, S. Miao, Y. Zhang, L. Chen, Dry heating and annealing treatment synergistically modulate starch structure and digestibility, Int. J. Biol. Macromol. 137 (2019) 554–561, https://doi.org/10.1016/j.ijbiomac.2019.06.137.
[25] V.P. Yuryev, A.V. Krivandin, V.I. Kiseleva, L.A. Wasserman, N.K. Genkina, J. Fornal, W. Blaszczak, A. Schiraldi, Structural parameters of amylopectin clusters and semi-crystalline growth rings in wheat starches with different amylose content, Carbohydr. Res. 339 (16) (2004) 2683–2691, https://doi.org/10.1016/j.carres.2004.09.005.
[26] T. Suzuki, A. Chiba, T. Yano, Interpretation of small angle X-ray scattering from starch on the basis of fractals, Carbohydr. Polym. 34 (4) (1997) 357–363, https://doi.org/10.1016/s0144-8617(97)00170-7.
[27] G. Beaucage, Approximations leading to a unified exponential/power-law approach to small-angle scattering, JApCr 28 (6) (1995) 717–728, https://doi.org/10.1107/S0021889895005292.
[28] A.J. Hurd, W.L. Flower, In situ growth and structure of fractal silica aggregates in a flame, J. Colloid Interface Sci. 122 (1) (1988) 178–192, https://doi.org/10.1016/0021-9797(88)90301-3.
[29] B.S. Hsiao, R.K. Verma, A novel approach to extract morphological variables in crystalline polymers from time-resolved synchrotron SAXS data, J. Synchrotron Radiat. 5 (1) (1998) 23–29, https://doi.org/10.1107/S0909049597010091.
[30] M.B. Cardoso, H. Westfahl, On the lamellar width distributions of starch, Carbohydr. Polym. 81 (1) (2010) 21–28, https://doi.org/10.1016/j.carbpol.2010.01.049.
[31] B. Zhang, F. Xie, D.K. Wang, S. Zhao, M. Niu, D. Qiao, S. Xiong, F. Jiang, J. Zhu, L. Yu, An improved approach for evaluating the semicrystalline lamellae of starch granules by synchrotron SAXS, Carbohydr. Polym. 158 (2017) 29–36, https://doi.org/10.1016/j.carbpol.2016.12.002.
[32] W. Situ, L. Chen, X. Wang, X. Li, Resistant starch film-coated microparticles for an oral colon-specific polypeptide delivery system and its release behaviors, J. Agric. Food Chem. 62 (16) (2014) 3599–3609, https://doi.org/10.1021/jf500472b.
[33] N. Li, Z. Cai, Y. Guo, T. Xu, D. Qiao, B. Zhang, S. Zhao, Q. Huang, M. Niu, C. Jia, L. Lin, Q. Lin, Hierarchical structure and slowly digestible features of rice starch following microwave cooking with storage, Food Chem. 295 (2019) 475–483, https://doi.org/10.1016/j.foodchem.2019.05.151.
[34] E. Cameron Ruth, M. Donald Athene, A small-angle X-ray scattering study of starch gelatinization in excess and limiting water, J. Polym. Sci. B Polym. Phys. 31 (9) (1993) 1197–1203, https://doi.org/10.1002/polb.1993.090310914.
[35] D. Qiao, F. Xie, B. Zhang, W. Zou, S. Zhao, M. Niu, R. Lv, Q. Cheng, F. Jiang, J. Zhu, A further understanding of the multi-scale supramolecular structure and digestion rate of waxy starch, Food Hydrocoll. (2016) https://doi.org/10.1016/j.foodhyd.2016.10.041.
[36] R. Hoover, Starch retrogradation, Food Rev. Int. 11 (2) (1995) 331–346, https://doi.org/10.1080/87559129509541044.
[37] M.A. Del Nobile, T. Martoriello, G. Mocci, E. La Notte, Modeling the starch retrogradation kinetic of durum wheat bread, J. Food Eng. 59 (2) (2003) 123–128, https://doi.org/10.1016/S0260-8774(02)00441-7.
[38] M. Li, S. Dhital, Y. Wei, Multilevel structure of wheat starch and its relationship to noodle eating qualities, Crit. Rev. Food Sci. Nutr. 16 (5) (2017) 1042–1055, https://doi.org/10.1111/1541-4337.12272.
[39] H. Wang, Y. Liu, L. Chen, X. Li, J. Wang, F. Xie, Insights into the multi-scale structure and digestibility of heat-moisture treated rice starch, Food Chem. 242 (2018) 323–329, https://doi.org/10.1016/j.foodchem.2017.09.014.
[40] Y. Liu, L. Chen, H. Xu, Y. Liang, B. Zheng, Understanding the digestibility of rice starch-gallic acid complexes formed by high pressure homogenization, Int. J. Biol. Macromol. 134 (2019) 856–863, https://doi.org/10.1016/j.foodchem.2017.09.014.
[41] H. He, C. Chi, F. Xie, X. Li, Y. Liang, L. Chen, Improving the in vitro digestibility of rice starch by thermomechanically assisted complexation with guar gum, Food Hydrocoll. 102 (2020), 105637. https://doi.org/10.1016/j.foodhyd.2019.105637.